Accurate determination of the spherical aberration coefficient of a FEG electron microscope using digital electron micrographs*

REN Gang (任 罡)**, DUAN, Xiaofeng (段晓峰) and PENG Lianmao (彭练矛)

(Beijing Laboratory of Electron Microscopy, Chinese Academy of Sciences, Beijing 100080, China)

Received August 30, 1996

Abstract It is shown that for a weak phase object the image formation process in a FEG electron microscope is the same as in a conventional transmission electron microscope, and that the spherical aberration coefficient of a FEG electron microscope may be measured by using an amorphous thin film. Methods were developed for accurate determination of the spherical aberration coefficient of a FEG electron microscope using digital electron micrographs.

Keywords: spherical aberration coefficient, FEG electron microscope, digital electron micrograph, FFT

The spherical aberration of the objective lens of an electron microscope strongly influences the image formation of the electron microscope. The accurate determination of the spherical abgerration coefficient C_s is therefore of crucial importance to many applications of electron microscopy techniques, including electron holography[1, 2], image processing and deconvolution[3], and electron crystallography of proteins[4].

The spherical aberration coefficient C_s of an electron microscope may in principle be determined either by using the Krivanek[5], statistic method[6] or beam-tilt method[7]. Usually films are employed in recording electron micrographs and then digitized when accurate digital data are required. A more efficient route for these types of studies is to use the recently developed slow-scan charge-coupled device (SSCCD) camera system. The use of SSCCD has led to the development of a new branch of electron microscopy-quantitative electron microscopy (QEM). Digitally recorded high resolution electron microscopy (HREM) images and diffraction patterns are more suited for off-line processing and comparison with theoretical calculations. Using digital convergent beam electron diffraction (CBED) patterns, low order structure factors in a crystal have been determined to a high accuracy[8—10]. Using digital HREM images combined with image processing techniques, detailed crystal structure information has been obtained directly[3]. In this paper we will be concerned with the determination of the spherical aberration coefficient of a field-emission gun (FEG) electron microscope newly installed in our laboratory. In sec. 1 we will first examine the image formation processes in a FEG electron microscope and then in sec. 2 discuss the basic principles behind the various methods for the determination of C_s. In sec. 3 we will present a FFT based data interpolation technique and in sec. 4 methods for improving statistics of digital

* Project supported by the National Natural Science Foundation of China.

** Also with Department of Material Physics, Beijing University of Science and Technology, Beijing 100083.

electron micrographs. In sec. 5 we will give some details of our procedure for the determination of C_s and comparison with conventional method and our conclusions will be given in section 6.

1 Image formation in an FEG electron microscope

From the viewpoint of image formation, an electron microscope is best represented by a contrast transfer function (CTF). For a perfect coherent illumination this CTF is represented as $t(u; Z)$ in reciprocal space as[12]

$$t(u; Z) = A(u)\exp\{i\chi(u; Z)\}, \tag{1}$$

in which $A(u)$ is the aperture function describing the effect of the objective aperture and is given by

$$A(u) = \begin{cases} 1, & \text{if } u \text{ lies inside the objective aperture} \\ 0, & \text{otherwise,} \end{cases}, \tag{2}$$

and $\chi(u; Z)$ describes the combined effects of the defocus and spherical aberration

$$\chi(u; Z) = \pi Z\lambda u^2 + \frac{1}{2}\pi C_s\lambda^3 u^4,$$

where Z is the defocus value, C_s is the spherical aberration coefficient, and λ is the wavelength of the incident electron wave.

Assuming on the image plane of an electron microscope the electron wave function is given by $\psi(x)$ in real space and $\varphi(u)$ in reciprocal space, these two functions are then related to each other via the standard Fourier transform

$$\varphi(u) = \int \psi(x)\exp(2\pi i u \cdot x)\mathrm{d}x. \tag{4}$$

In reciprocal space the electron wave function $\varphi(u)$ is related to that on the exit face of the crystal $\varphi_E(u)$ via the relation:

$$\varphi(u) = \varphi_E(u)t(u; Z). \tag{5}$$

The Fourier transform of the image intensity distribution is called the diffractogram of the image. Using eq. (4) we have

$$\begin{aligned} J(u; Z) &= \int \psi(x)\psi^*(x)\exp(2\pi i u \cdot x)\mathrm{d}x \\ &= \int du'\varphi_E(u + u')\varphi_E^*(u')T(u + u', u'; Z), \end{aligned} \tag{6}$$

in which $T(u + u', u'; Z)$ is called the transmission cross-coefficient (TCC) and under the usual approximations for an electron microscope[14] is given by

$$T(u+u',\ u';\ Z) = A(u+u')A(u')\exp\{i[\chi(u+u';\ Z) - \chi(u';\ Z)]\}. \quad (7)$$

We now consider the effects of a finite sized electron source and the defocus fluctuations due to either the finite energy distribution of the electron source or the relative instabilities of the objective lens current, For a conventional transmission electron microscope (CTEM), images formed with different defocus and electrons emitted from different positions of the electron source may be regarded as incoherent. The resultant image is then given by an average of a set of images of different angles of incidence and defocus values. Assuming $B(s)$ and $f(Z)$ are the normalized intensity of the electron source and defocus distribution, an appropriate average gives

$$\langle J(u)\rangle = \iint dsdZB(s)f(Z)J(u,\ sZ), \quad (8)$$

Here we have changed the notation $J(u;\ Z)$ to $J(u,\ s;\ Z)$ to emphasize explicitly that the function depends on the incident beam direction s.

For an FEG electron microscope since the electron source size is very small, the condenser aperture in the microscope may be regarded to be filled coherently. Given the same normalized intensity distribution function $B(s)$ for the electron source as for a CTEM, we have the following average wave function rather than average intensity

$$\langle\varphi(u;\ Z)\rangle = \int dsB(s)\varphi_E(u,\ s)t(u+s;\ Z), \quad (9)$$

and hence an average intensity

$$\langle I(x;\ Z)\rangle = |\langle\varphi(u;\ Z)\rangle|^2. \quad (10)$$

The effect of the defocus fluctuations on the image may be treated as for a CTEM, and the average image intensity is given by

$$\langle J^{FEG}(u)\rangle = \int dZ'f(Z')\mathcal{F}\{|\langle I(x;\ Z+Z')\rangle|^2\}. \quad (11)$$

Following Frank[14] and Wade and Frank[15], we denote both the effective source intensity distribution and the defocus spread distribution by the normalized Gaussian forms:

$$B(s) = \frac{1}{\pi s_0^2}\exp\left\{-\frac{s^2}{s_0^2}\right\},\ f(Z') = \frac{1}{\sqrt{\pi}\Delta}\exp\left\{-\frac{Z'^2}{\Delta^2}\right\}. \quad (12)$$

To simplify our discussion even futher, we note that for most electron microscopes, s_0 and Δ are very small and the wave aberration $\chi(u+s;\ Z+Z')$ may be expanded in the neighborhood of u and Z

$$\chi(u+s;\ Z+Z') = \chi(u;\ Z) + s\cdot\nabla\chi(u;\ Z) + Z'\frac{\partial\chi(u;\ Z)}{\partial Z}, \quad (13)$$

where $\nabla\chi(u;\ Z)$ stands for the gradient of the wave aberration function $\chi(u;\ Z)$. Substitution

of eqs (12) and (13) into eq. (11) gives

$$\langle J^{FEG}(\chi)\rangle = \int du' \varphi_E(u+u')\varphi_E(u') T^{FEG}(u+u', u'; Z), \tag{14}$$

in which

$$T^{FEG}(u, u'; Z) = A(u)A(u')\exp\{i[\chi(u; Z) - \chi(u'; Z)]\} E_s^{FEG}(u, u'; Z) E_f(u, u'), \tag{15}$$

with

$$E_s^{FEG}(u, u'; Z) = \exp\left\{-\frac{1}{4}s_0^2[\,|\nabla\chi(u; Z)|^2 + |\nabla\chi(u; Z)|^2]\right\}$$

$$= \exp\{-\pi^2 s_0^2\lambda^2[(Z + C_s\lambda^2 u^2)u^2 + (Z + C_s\lambda^2 u'^2)u'^2]\}. \tag{16}$$

and

$$E_f(u, u) = \exp\left\{-\pi^2\Delta^2\left[\frac{\partial}{\partial z}\chi(u; Z) - \frac{\partial}{\partial z}\chi(u'; Z)\right]^2\right\}$$

$$= \exp\left\{-\left(\frac{\pi\Delta\lambda}{2}\right)^2[u^2 - u'^2]^2\right\}. \tag{17}$$

For a CTEM, E_f due to the defocus fluctuation is the same as that for a FEG electron microscope, E_s due to the finite incident beam convergence is different and is given by[13]

$$E_s(u, u'; Z) = \exp\left\{-\frac{1}{4}s_0^2[\nabla\chi(u; Z) - \nabla\chi(u'; Z)]^2\right\}$$

$$= \exp\{-\pi^2 s_0^2\lambda^2[(Z + C_s\lambda^2 u^2)u^2 + (Z + C_s\lambda^2 u'^2)u'^2]\}. \tag{18}$$

It should be noted, however, that the following equalities hold between E_s for a CTEM and E_s^{FEG} for a FEG electron microscope

$$E_s^{FEG}(u, 0; Z) = E_s(u, 0; Z),\ E_2^{FEG}(0, u; Z) = E_s(0, u; Z), \tag{19}$$

which leads to the following important relations

$$T^{FEG}(u, 0; Z) = T(u, 0; Z),\ T^{FEG}(0, u; Z) = T(0, u; Z). \tag{20}$$

In what follows we will show that these equalities ensure that for HREM images of weak phase objects the image formation processes are the same for both the FEG electron microscope and CTEM. The standard methods developed to measure the spherical aberration coefficient of a CTEM may then be applied directly to an FEG electron microscope.

For a thin film and a plane wave incidence, the exit electron wave function is given by[12]

$$\psi_E(x) = \exp\{i\sigma V(r)\}, \tag{21}$$

in which σ is called the interaction constant, $V(r)$ is the projected potential of the thin film in the incident beam direction. The weak phase object approximation assumes that the phase change introduced by the crystal potential is so small that a first order expansion may be made to equation (21)

$$\psi_E(x) \approx 1 + i\sigma V(r). \tag{22}$$

Fourier transform of $\psi_E(r)$ gives

$$\phi_E(u) = \delta(u) + iO(u), \tag{23}$$

where

$$O(u) = \sigma\mathcal{F}\{V(r)\}. \tag{24}$$

Substituting eq. (23) into eq. (14) and noticing that the crystal potential is a real quantity we then have

$$\langle J^{FEG}(u)\rangle = 1 + iO(u)[T^{FEG}(u, 0; Z) - T^{FEG}(0, -u; Z)]. \tag{25}$$

But from eq. (20) we know that $T^{FEG}(u, 0; Z) = T(u, 0; Z)$ and $T^{FEG}(0, -u; Z) = T(0, -u; Z)$. For a weak phase object we then have

$$\begin{aligned}\langle J^{FEG}(u)\rangle &= 1 + O(u)\sin[i\chi(u; Z)]\exp\left\{-\frac{1}{4}\pi^2\Delta^2\lambda^2u^4 - \pi^2s_0^2\lambda^2u^2(Z + C_2\lambda^2u^2)^2\right\} \\ &= \langle J(u)\rangle\end{aligned} \tag{26}$$

i.e. for the weak phase object approximation the diffractogram obtained using an FEG electron microscope is the same as that using a CTEM.

2 Basic principles for C_s determination

The basic idea behind the various methods for the measurement of C_s is to use a thin film of amorphous material. On the one hand a thin film may be regarded as a weak phase object, and on the other hand for an amorphous material we may make the following approximation

$$O(u) \approx C, \tag{27}$$

as in the case of a while nose. Using these approximations and considering only image contrast in a diffractogram, we obtain from eq. (26)

$$J_c(u) = \langle J(u)\rangle - 1 \approx C\sin[i\chi(u; Z)]E(u; Z), \tag{28}$$

in which E is just an envelope function representing combined effects of finite source size and defocus fluctuations

$$E(u; Z) = \exp\left\{-\frac{1}{4}\pi^2\Delta^2\lambda^2u^4\right\} \times \exp\{-\pi^2s_0^2\lambda^2u^2(Z + C_s\lambda^2u^2)^2\}. \tag{29}$$

Noticing that for an amorphous thin film the diffractogram is isotropic, eq. (28) clearly shows that a diffractogram will contain a ring pattern resulting from $\sin(i\chi)$ function, and the minima and maxima positions depend on both C_s and defocus value via $\chi(u; Z)$. For an electron micrograph taken under a defocus value $Z = \Delta f$, extremes in a diffractogram appearing at spatial frequency u satisfy

$$C_s\lambda^3 u^4 + 2\Delta f\lambda u^2 = n, \tag{30}$$

in which n is an integer number characterizing the order of the ring in a diffractogram. In principle a single diffractogram will be sufficient for determining both the defocus value Δf and C_s. Statistically speaking, a better method is to combine several diffractograms to reduce noise and errors. In the present study we have taken a through focus series of HREM images obtained from a thin film of amorphous silicon. These images were taken with equal focus shift such that for the j-th electron micrograph there is

$$\Delta f = f_0 + j\Delta f_0. \tag{31}$$

Using i to index the rings appearing in a diffractogram we have

$$C_s\lambda^3 u_{ij}^4 + 2\lambda(f_0 + j\Delta f_0)u_{ij}^2 = n_i. \tag{32}$$

Letting $A = C_s\lambda^3$, $B = 2\lambda f_0$ and $D = 2\lambda\Delta f_0$ be three fitting parameters, we define a merit function

$$\chi^2 = \sum_{i,j}[n_i - (Au_{ij}^4 + Bu_{ij}^2 + Dju_{ij}^2)]^2. \tag{33}$$

Defocus values f_0, Δf_0 and C_s can then be obtained by adjusting the fitting parameters A, B, D so that the χ^2 function is minimized. This minimization procedure is achieved in the present study by a general least-squares minimization procedure.

3 FFT based data interpolation

From our analysis presented in sec. 2, it is clear that the accuracy of C_s determination depends sensitively on the measurements of u_{ij} values, i.e. the ring positions in a diffractogram satisfying eq. (32). One major concern in dealing with digital electron micrographs is that the available number of pixels in a micrograph is usually rather limited and sometime may not be sufficient. Shown in fig. 1(a) is the central quarter of an diffractogram obtained directly via FFT the original HREM image of an amorphous silicon thin film. The diffractogram is then angularity averaged, and part of the resultant curve is shown in fig. 2 (dotted curve). It is seen that most of the peaks in the curve are ill-defined, and it will be shown later that direct use of this curve results in a rather large error bar over the determined value of C_s.

To improve this situation in this section we will briefly discuss an FFT based data interpolation method developed in our work. We will first consider a discrete real space image of $N \times N$ pixels such as the one obtained using a slow-scan CCD camera. Suppose that the size of one pixed in the CCD camera has a dimension of $d \times d$, and the distance between neighboring pixels is also

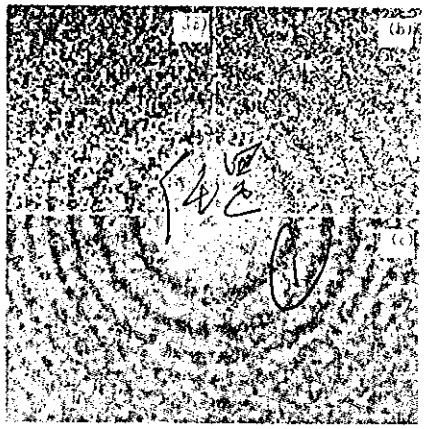

Fig. 1. Diffractogram obtained froma HREM image of an amorphous Silicon thin film using (a) tranditional FFT, (b) based interpolation method and (c) interpolation plus median filtering.

d. The intensity read out from one pixel having index (m, n) is therefore given by an integration of the intensity function $I(x, y)$ over the pixel

$$I_{m,n} = \frac{1}{d^2}\int_{(m-1)d}^{md}\int_{(n-1)d}^{nd} I(x, y)\mathrm{d}x\mathrm{d}y, \quad (34)$$

with $m, n = 1, \cdots, N$. It should be noted that $I_{m,n}$ obtained this way is slightly different from the value of the function $I(x, y)$ at the center of the pixel $\left(\left(m-\frac{1}{2}\right)d, \left(n-\frac{1}{2}\right)d\right)$. The discrete Fourier transform of I_{mn} is given by

$$J(u, v) = \frac{1}{N}\sum_{m,n=0}^{N-1} I_{m,n}\exp[2\pi i(um + un)d]. \quad (35)$$

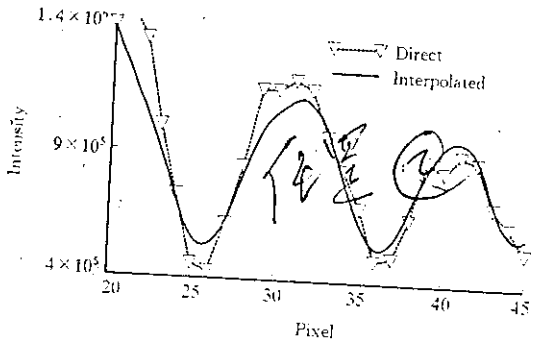

Fig. 2. Angular averaged diffractograms before and after interpolation (in relative unit).

Although eq. (35) may be used directly to calculate $J(u, v)$ at any coordinate in reciprocal space, a much more efficient method for calculateing discrete Fourier transform is to use FFT algorithm which can be used to calculate summation of the type:

$$J_{k,l} = \frac{1}{N}\sum_{m,n=0}^{N-1} I_{m,n}\exp[2\pi i(km + ln)/N], \quad (36)$$

with $-N/2 \leqslant k, l \leqslant N/2-1$. We will now show that this summation may readily be used to calculate the general expression (35) by some rearrangements. Suppose we can write (u, v) in reciprocal space as $(k+\Delta k, l+\Delta l)/(Nd)$, with $-1 \leqslant \Delta k, \Delta l \leqslant 1$ and $-N/2 \leqslant k, l \leqslant N/2-1$. Eq. (35) can then be rewritten as

$$F(k+\Delta k, l+\Delta l) = \frac{1}{N}\sum_{m,n=0}^{N-1} I_{m,n}\exp\{2\pi i[(k+\Delta k)m + (l+\Delta l)n]/N\} \quad (37)$$

$$= \frac{1}{N}\sum_{m,n=0}^{N-1}\{I_{m,n}\exp[2\pi i(\Delta km + \Delta ln)/N]\}\exp[2\pi i(km + ln)/N],$$

which is nothing but summation (36) except that now the real space function I_{mn} becomes $I_{mn}\exp\{-2\pi i(\Delta km + \Delta ln)/N\}$. Noticing that the new variables Δk, Δl permit a change in the display position in reciprocal space. An diffractogram obtained via direct FFT may therefore be inter-

polated into a higher resolution diffractogram having many more time data points than the original electron micrograph.

4 Median filtering and angular averaging

Although the FFT based data interpolation technique may be used to generate diffractograms revealing more details which are otherwise unobtainable form anordinary diffractogram, the signal-to-noise ratio of the diffractogram remains to be rather low (see fig. 1(b)). To overcome this difficulty we tested various types of filters to improve the signal-to-noise ratio of the diffractogram and found that the so-called median filter[11] provides rather satisfactory result as shown in fig. 1(c).. This filter is a typical low-pass filter that is best suited for reducing noise, but at the same time without losing a lot of details of the original images. Since now we are equipped with a device via which we can increase sampling points in the reciprocal space indefinitely as we wish, the loss of resolution in the reciprocal space by the median filtering can always be compensated by an increase in the data points or sampling rate in reciprocal space. A further improvement is provided by an angular average of the diffractogram. Shown in figs. 2 (dark line) and are curves of angular average of the diffractogram following an application of the median filter to the original electron micrograph. When compared with the dotted line in fig. 2 which is obtained without data interpolation and median filtering, the improvement in the statistics of the curve is seen to be substantial.

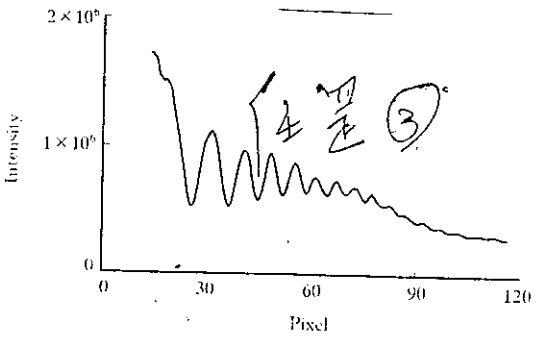

Fig. 3. Angular averaged diffractogram obtained from a median filtered diffractogram which has been interpolated with 16 times more data points (in relative unit).

5 Experiment procedure and results

The experiment was performed on a Philips CM200-FEG electron microscope equipped with a gatan imaging filter (GIF). The microscope is computer controllable by means of a serial port. The images were recorded with a Gatan slow scan CCD camera. A thin foil of Si(110) was made by ion-milling. A thin area of amorphous silicon is produced around the edge of the film during ion-milling, and is used for measuring C_s. Our procedure consists of the following steps:

(ⅰ) Take a through focus series of HREM images from a thin amorphous film of silicon. The CCD camera size used is 512×512. The magnification of these HREM images are calibrated using an HREM image taken from the same sample but from a different area with a region of perfect Si single crystal along [110] zone axis.

(ⅱ) Calculate the high resolution diffractograms of the digital HREM images obtained in step 1 using the FFT based data interpolation technique 9see fig. 1(b)). Usually 16 times more data points are added to the original diffractograms.

(ⅲ) Median filtering and angular averaging all diffractograms obtained in step (ⅲ) and find

all values of u_{ij} satisfying equation (32).

(Ⅳ) Determine C_s and calculate associated standard deviation using a general non-linear least-squares method.

Using the above procedure, we have determined C_s value of our CM200-FEG electron microscope. A total of 24 HREM images were used in the procedure. C_s was determined by two methods, and our results are given in table 1. These data clearly show that results obtained by the method discussed in this paper is much superior to and more reliable than the conventional method. To further illustrate this point we drau in fig. 4 the distribution of deviations between the theoretical and experiment values of maxima and minima in the diffractograms. In the figure the theoretical values were calculated using the determined values of C_s and Δf. The distribution shown in fig. 4(a) was obtained using the conventional method, and fig. 4(b) was obtained using the present method. This figure shows clearly that the half-width of the distribution for the present method is smaller than that for the conventional method, indicating that results obtained using our method is much more reliable.

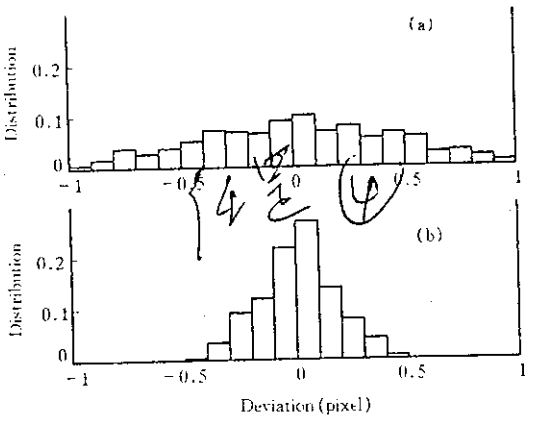

Fig. 4. Distribution of deviation between the theoretical and experimental maxima and minima for (a) an ordinary diffractogram and (b) a filtered and interpolated diffractogram.

Table 1 Determined fitting parameters and associated standard deviations using conventional FFT based (FFT) and present FFT interpolation based (FFTI) methods

	C_s	$\sigma(C_s)$	Δf_0	$\sigma(\Delta f_0)$	f_0	$\sigma(f_0)$
FFT	1.327 mm	0.239 mm	−8.116 nm	0.289 nm	−208.558 nm	8.381 m
FFTI	1.245 mm	0.045 mm	−8.099 nm	0.208 4 nm	−205.835 nm	5.010 nm

6 Conclusions

We have shown in this paper that for weak phase object the contrast transfer function of an FEG electron microscope is the same as that of a conventional transmission electron microscope, and the usual method of measuring the spherical aberration coefficient of an electron microscope is applicable to the case of an FEG electron microscope. In applying the conventional method to measure the spherical aberration coefficient of a newly installed FEG CM200 electron microscope in our laboratory using digital electron micrographs, we found two major difficulties, i.e. the signal-to-noise ratio is usually rather unsatisfactory and that the digital micrographs do not have sufficient pixels to allow an accurate determination of the spherical aberration coefficient. To overcome the former difficulty various filters have been tested and evaluated, and we have found that a median filter gives rather improved signal-to-noise ratio and at the same time this filter preserves all necessary details of the original electron micrographs. We have also developed an FFT based data interpolation technique. By using this technique we are able to increase indefinitely the number of pixels in a digital diffractogram. The combination of our data interpolation and the median

filtering techniques enables us to determineaccurately the spherical aberration coefficient of our new FEG electron microscope to be $C_s = (1.245 \pm 0.045)$ mm using the method of leastsquare fitting, and this C_s value corresponds to a point resolution of 0.247 nm.

References

1 Lichte, H., Parameters for high-resoution electron holography, *Ultramicroscopy*, 1993, 51: 15.
2 Peng, L.-M., Ren, G., Duan, X. F., Sampling theorem and digital electron microscopy, *J. Chinese Electron Microscopy Society* (in Chinese), 1996, 15(2—4): 117.
3 Li, F. H., Combination of high resolution electron microscopy and electron diffraction in crystal structure determination, *J. Chin. Electr. Microsc. Soc.*, 1996, 1592—4): 143.
4 Baumeister, W, Typke, D., Electron Crystallography of Proteins: State of the Art and Strategies for the Future, *MSA Bulletin*, 1993, 23(1): 11.
5 Krivanek, O. L., A method for determining the coefficient of spherical aberration from a single electron micrograph, *Optik*, 1976, 45(1): 97.
6 Coene, W. M. J., Deneteneer, T. J. J., Improved methods for the determination of the spherical aberration coefficient in high-resolution electron microscopy from micrographs of an amorphous object, *Ultramicroscopy*, 1991, 38: 225.
7 Koster, A. J., de Jong, A. J., Measurement of the spherical aberration coefficient of transmission electron microscopes by beam-tilt-induced image displacements, *Ultramicroscopy*, 1991, 38: 235.
8 Saunders, M., Bird, D. M., Zaluzec, N. J., et al., Measurement of low-order structure factors for silicon from zone-axis CBED patterns, *Ultramicroscopy*, 1995, 60: 311.
9 Peng, L.-M., Zuo, J. M., Direct retrieval of crystall structure factors in THEED, *Ultramicroscopy*, 1995, 57: 1.
10 Spence, J. C. H., Zuo, J. M., *Electron Microdiffraction*, New York: Plenum, 1992.
11 Gonzalez, R. C., Woods, R. E., *Digital Image Processing*, Addison-Wesley: Reading, 1993, p191.
12 Cowley, J. M., *Diffraction Physics*, Horth-Holland: Amsterdam, 1990.
13 Ishizuka, K., Contrast transfer of crystal images in TEM, *Ultramicroscopy*, 1980, 5: 55.
14 Frank, J., The envelope of electron microscopic transfer functions for partially coherent illumination, *Optik*, 1973, 38: 519.
15 Wade, R. H., Frank, J., Electron microscope transfer functions for partially coherent axial illumination and chromatic defocus spread, *Optik*, 1977, 49: 81.